Original Research

Probing Metal Ion Interactions in Stacked Polycyclic Aromatic Hydrocarbons as a Molecular Model for Superconductivity

Exploration des interactions métallique-ion dans les hydrocarbures aromatiques polycycliques empilés comme modèle moléculaire de la supraconductivité

Victor Lee[1], Olivia Chen[2], Natasha Saltarelli[1], Paul Mayer[1*]

1. University of Ottawa, Ottawa, ON, Canada
2. Merivale High School, Ottawa, ON, Canada
*Corresponding author. Email: pmmayer@uottawa.ca

Abstract | Résumé

Metal ion intercalated graphene has been shown to display superconductive properties. Most metals chosen for intercalation are alkali and alkaline earth metals. This study explores the intercalation of graphene with nickel as a more environmentally-friendly alternative. As a first step, the matrix-assisted laser desorption ionization was used to study the structure of the dimer of coronene intercalated with a Ni atom. The ions were formed by laser desorption from a target containing a mixture of coronene and Ni salt, the dimer ion with m/z 657 was selected, and the collision-induced dissociation mass spectrum was obtained with the LIFT technology on our Bruker MALDI-TOF/TOF. The results showed that the dimer dissociated by H-atom transfer from a coronene molecule to Ni. This was supported by density functional calculations of the reaction energetics. The results suggest that the laser desorption process leads to a cluster ion better described as an ionic complex between CorNiH and Cor-H, rather than a formal [$(Cor)_2Ni$] ion.

———

Il a été démontré que le graphène intercalé aux ions métalliques présente des propriétés supraconductrices. La plupart des métaux choisis pour l'intercalation sont des métaux alcalins et alcalino-terreux. Cette étude explore l'intercalation du graphène avec le nickel comme alternative plus respectueuse de l'environnement. En première étape, l'ionisation laser assistée par matrice a été utilisée pour étudier la structure du dimère de coronène intercalé avec un atome de Ni. Les ions ont été formés par désorption laser à partir d'une cible contenant un mélange de coronène et de sel de Ni, l'ion dimère avec m/z 657 a été sélectionné, et le spectre de masse de dissociation induit par collision a été obtenu avec la technologie LIFT sur notre Bruker MALDI-TOF/TOF. Les résultats ont montré que le dimère se dissocie par transfert d'atome d'H d'une molécule coronène vers Ni. Cela était soutenu par des calculs de la fonction de densité de l'énergétique de réaction. Les résultats suggèrent que le processus de désorption laser conduit à un ion cluster mieux décrit comme un complexe ionique entre CorNiH et Cor-H, plutôt qu'un ion formel [$(Cor)_2Ni$].

Keywords: superconductivity; graphene intercalation; coronene; polycyclic aromatic hydrocarbons; nickel intercalation; MALDI-TOF/TOF; collision-induced dissociation; density functional theory; graphite intercalation compounds; host–guest interactions

Introduction

Superconductivity is a quantum mechanical phenomenon that allows materials to conduct electricity without resistance and expel magnetic fields when cooled to below a specific critical temperature (T_c) (1). It has been found that the superconducting state was not only related to temperature but also to the current in the superconductor and the applied external magnetic field. These three effects have limited the practical application of many superconducting materials (2). There is an ongoing quest for higher-temperature superconductors from practical materials that challenge these limitations. Recent advances include carbon-based superconductors that have been developed through intercalation chemistry and carrier doping techniques (3). Intercalation refers to the insertion of guest species (atoms, ions, molecules) into the spaces between layers of a host material framework without majorly disrupting its molecular framework. This occurs in highly anisotropic structures where intraplanar binding forces are larger than interplanar binding forces (4). Doping refers to the addition or substitution of impurity guest species into a material, altering its lattice structure in the process. These techniques provide the host molecule a means for varying several physical properties over wide ranges, depending on the type and degree of intercalation or doping.

Graphene (Figure 1a) can present superconductivity upon metal ion intercalation and doping (5). Intercalation is particularly interesting as it presents the opportunity to tune material electronic properties (6). Graphite intercalation compounds (GICs) are materials that are formed by inserting guest species between graphitic layers without disrupting the planar hexagonal carbon framework. In 1965, superconductivity was observed in

K-intercalated graphite (KC_8) (7). Interestingly, no superconductivity was observed in KC_{24} or KC_{36}, which suggests that the alternating arrangement of metal and graphene layers is critical for superconductivity to be observed in GICs. This highlights the fundamental importance of the structure-property relationship of these materials.

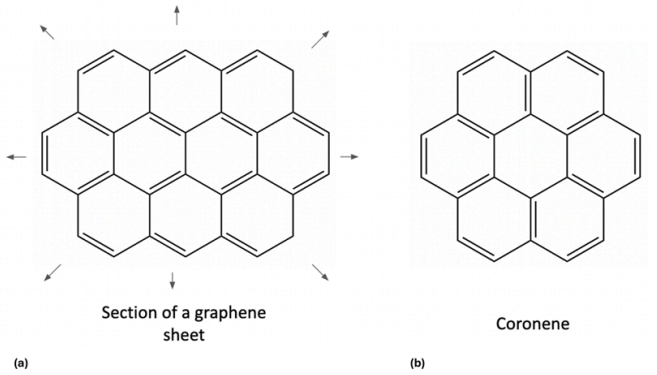

Figure 1. (a) Structure of a section of a graphene sheet, and (b) Structure of coronene

After this discovery, Ca intercalated graphite was discovered, with a T_c as high as 11.5K in CaC_6 (8). The tunability of GICs, through control over staging (number of graphene layers between intercalant layers), type of intercalation, and concentration of intercalant, makes them ideal platforms for probing electronic effects in layered carbon systems.

Since the discovery of graphene-based superconductors, experimental measurements of their binding patterns have relied on assumptions and often yielded contradictory results (9). While the average structures of the bulk material have been studied, investigating the intercalant binding patterns at specific sites remains challenging. Metal binding to graphitic sheets can occur in various forms, including direct intercalation between layers, surface functionalization, or edge binding between sheets. These distinct binding patterns can significantly influence the material's electronic properties. Previous studies of GICs have employed techniques such as X-ray diffraction and electron diffraction; however, these methods have limited spatial resolution, which affects characterization at the atomic level (10). This creates challenges in studying GIC's binding systems and the properties that arise from them. A potential solution to the study of graphene's molecular properties can be found using polycyclic aromatic hydrocarbons (PAHs) as molecular models of graphene, since they can be viewed as fragments of graphene sheets. Their extensive π-molecular orbitals allow electrons to become delocalized, leading to characteristics of conductivity (11). Although it is very different in size than graphene, heteroatom-intercalated PAHs, such as coronene (Figure 1b) could yield valuable information on the graphene system (12,13).

The objective of the study is to determine the type of metal binding that can occur on coronene and in coronene dimers (14,15), using matrix-assisted laser desorption ionization (MALDI) time-of-flight (TOF) mass spectrometry and theory. While Li has been employed extensively in GICs due to the mobility of Li in the lattice, it is a rare metal whose extraction has significant environmental cost. Thus, we decided to investigate a more common metal, nickel, that also has economic advantages for the Canadian economy, to see if it has desirable intercalation properties.

Methods

MALDI-TOF Mass Spectrometry

All chemicals were obtained from MilliporeSigma (Oakville, ON) and used without further purification. For MALDI-TOF, 3 mg of nickel chloride salt was dissolved in 1 ml of a solvent comprised of 50:50 (v/v) acetonitrile and water. 10 mg of coronene was dissolved separately in 1 ml of chloroform. 25µl of each solution was deposited into a glass vial and sonicated until homogeneous. The dried-droplet spotting method was employed, which involves depositing 1 µl spots of the prepared solution onto the surface wells of the Bruker MTP 384 ground steel plates and drying under ambient conditions. Mass spectra were acquired using a Bruker ultrafleXtreme MALDI-TOF/TOF reflecting mass spectrometer in positive-ion mode, covering a mass range of m/z 0-1200. Laser desorption was achieved via a frequency-tripled Nd:YAG laser at a wavelength of 337 nm and a pulse rate of 1000 Hz. Tandem mass spectrometry was performed using the LIFT functionality on the instrument. High-resolution MS peaks corresponding to the precursor ion of interest were selected with a PCIS (precursor ion selection) window of 2 Da.

Computational Procedures

Geometry optimization and vibrational frequency calculations employing the M06/6-31+G(d) level of theory were performed with the GAUSSIAN 16 suite of programs (16).

Results and Discussion

Coronene-nickel clusters were observed using MALDI-TOF. Figure 2 showcases the coronene-nickel monomer and dimer clusters at their respective m/z range. The clusters were confirmed using isotope distribution models, which accounted for the natural abundances of carbon and nickel isotopes.

The dissociation of the coronene-nickel complex ion with m/z 358 showed one fragment ion at m/z 299, corresponding to a coronene fragment with hydrogen loss ($[Cor\text{-}H]^+$), Figure 3a. The only possible pathway that explains this peak is the loss of a neutral 59 Da fragment corresponding to NiH. The hydrogen transfer was also seen for the sodium cluster on ESI-MS. The absence of further fragmentation products implies that the coronene skeleton is intact, reinforcing its stability under LIFT conditions and the lack of sequential fragmentation events. The LIFT mass spectrum for the $(Cor)_2Ni^+$, m/z 658, is shown in Figure 4b. There are three notable fragment peaks at m/z 299, 357, and 359. The peak at m/z 308 may be the result of a C_4H_2 loss to form a stable corannulene intermediate ($C_{20}H_{10}^+$) with Ni coordination. However, this is highly

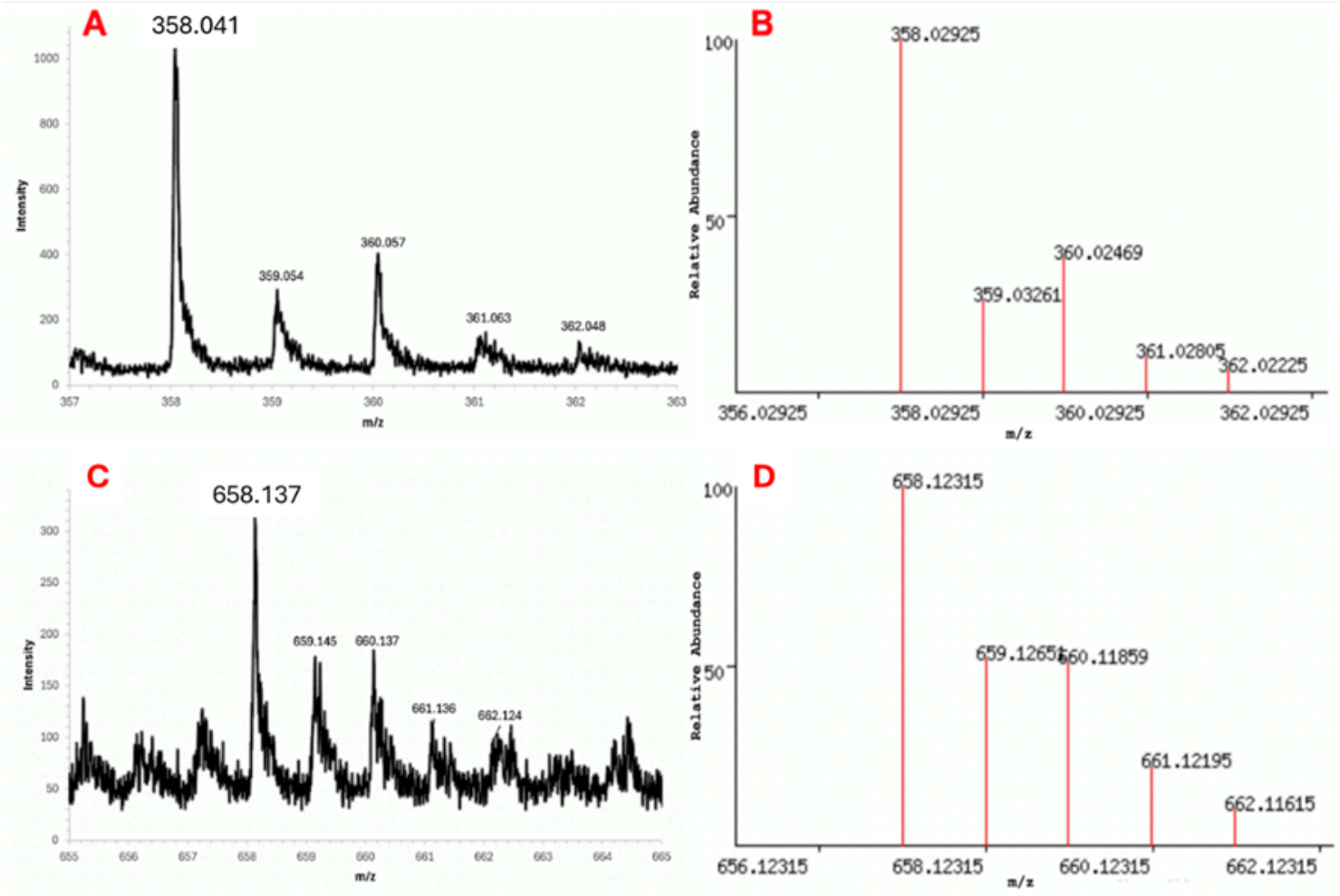

Figure 2. A) MALDI-TOF mass spectrum of coronene-nickel monomer cluster $[C_{24}H_{12}Ni]^+$ B) isotope distribution model of the monomer, C) Mass spectrum of the coronene-nickel dimer cluster $[(C_{24}H_{12})_2Ni]^+$, and D) isotope distribution model of the dimer cluster.

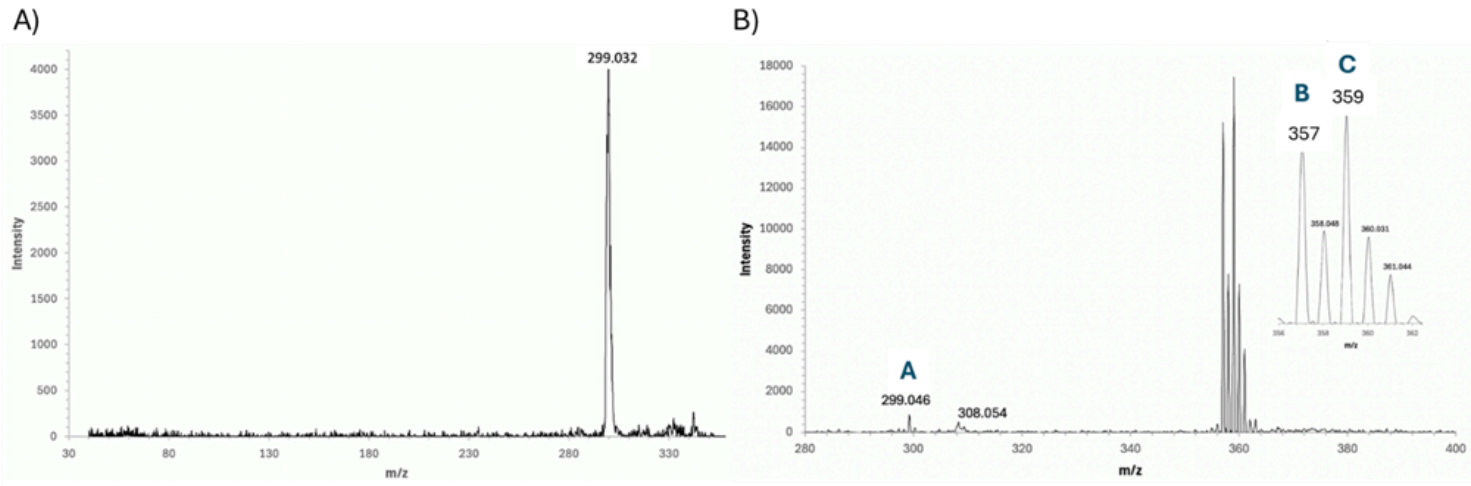

Figure 3. MALDI LIFT TOF/TOF mass spectrum A) [(Cor)Ni]+ and B) of the dimer cluster ($[(Cor)_2Ni]^+$), with an expansion of the m/z 357-361 region in the inset. Blue labels are referred to in the text.

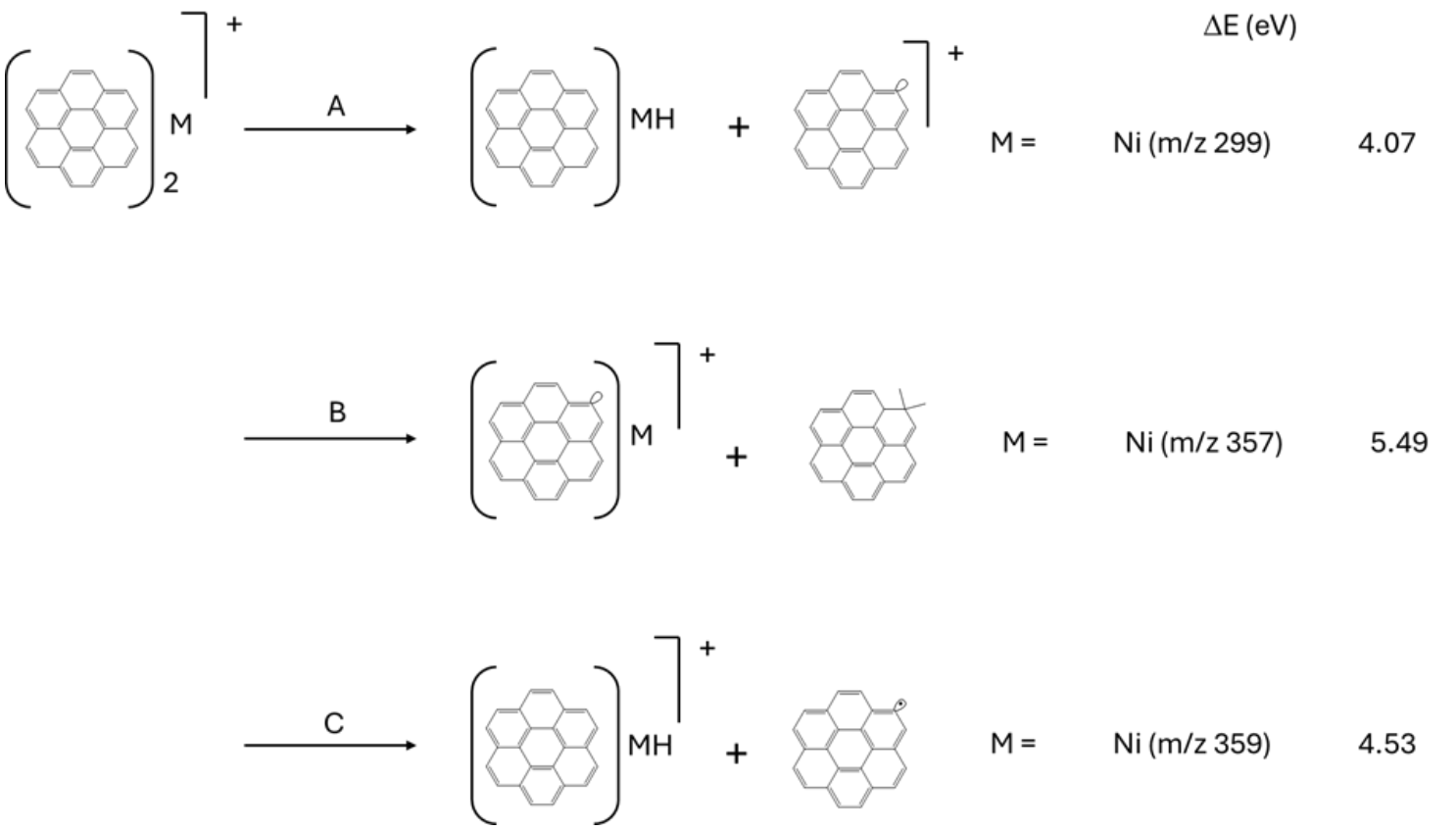

Figure 4. Summary of the experimentally observed dissociation reactions of the $[(Cor)_2M]^+$ system, where M = Na and/or Ni. Calculated M06/6-31+G(d) energies (relative to the respective dimer ions) are shown for the two metals.

speculative as C_4H_2 loss is an uncommon loss channel in PAH ions (17).

The isotope distribution of the series of peaks from m/z 357-361 does not match the isotope distribution of the obvious $C_{24}H_{11}Ni^+$ fragment; the intensity of the peak at 359 is too high. Therefore, it is likely that two fragments contribute to this series of peaks: $[C_{24}H_{11}Ni]^+$ and $[C_{24}H_{12}NiH]^+$. This suggests the presence of three competing dissociation pathways labelled A-C in Figure 4b. Reaction A has the Ni abstracting an H atom from a coronene ring before the complex splits to form m/z 299. Reaction C is the complementary reaction in which the ion charge is retained on the coronene/NiH fragment. Reaction B is the splitting of the dimer complex with H-atom transfer to the departing neutral coronene ($C_{24}H_{13}$). The observed reactions are summarized in Figure 4.

Computational Study

The most stable dimer ion was found to be the sandwich structure with the Ni atom between two coronene rings (Figure 5). For $[(Cor)_2Ni]^+$,Mulliken partial charges show the charge to be split between the organic ring and Ni atom due to the similarity in the two ionization energies (IE), 7.68 eV (Ni) (18) vs 7.29 eV for coronene (19). The M06/6-31+G(d) relative product energies are summarized in Figure 4. Structures for each species in Figure 4 are shown in Figure 5.

Interestingly, the calculated binding energy for the dimer (relative to $[CorNi]^+$ + Cor) is a scant 0.1 eV. This suggests that these ions are not made during the laser desorption stage of the experiment, as they would not survive to the LIFT process for CID, and there is definitely no m/z 300 or 358 peak in the LIFT spectra. Insight into the structure of these ions comes from the observed mass spectra.

For the ions formed in pathways B ($[(Cor-H)Ni]^+$) and C ($[CorNiH]^+$)

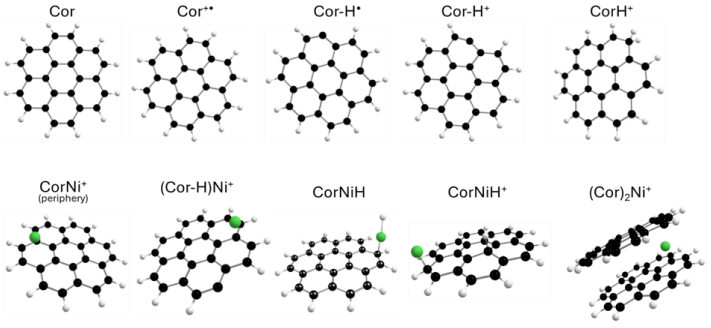

Figure 5. Structures of species in Figure 4, calculated at the M06/6-31+G(d) level of theory.

of the Ni system, the Mulliken analysis reveals that the positive charge is primarily localized on the nickel atom. Upon metal coordination, nickel is the electron-deficient atom that preferentially carries the positive charge in these systems. Through this interpretation, pathway A leading to the metal-absent ion is energetically higher because there is an unfavourable charge transfer from the nickel to the coronene. A similar conclusion was reached by Pozniak and Dunbar, as a similar unfavourable charge transfer process was thought to compete with coronene-metal ion cluster formation for the reaction of the bare metal ion onto the monomer cluster (14).

The formation of a Ni–H bond in pathway C leads to a slightly delocalized positive charge on the nickel atom. The hydride is an electron-rich ligand that can donate electron density towards the metal center, leading to a lower partial positive charge. In pathway B, the partial charge of the metal center is higher due to the absence of any electron-donating ligands. This interpretation is supported by the Mulliken charge data, which shows a higher partial charge on the nickel atom in pathway B (+0.92) compared to pathway C (+0.90). The lower partial positive charge in the ion produced from pathway C due to the hydride ligand may be a factor contributing to its higher reaction energy. It is also possible that hydrogen transfer between the coronene complexes in pathway B presents a lower energy transition state.
The results suggest that the laser desorption process leads to a cluster ion better described as an ionic complex between CorNiH and Cor-H, rather than a formal $[(Cor)_2Ni]$ ion.

Conclusion

H-abstraction by the metal ion is a common observation in the CID of $[(Cor)_2Ni]^+$. Density functional theory calculations of the energetics support the observation of the major kinetic pathways. The formation of the kinetic product ions strongly suggests that the nickel atom is intercalated between the coronene molecules, as the formation of these ions is energetically improbable in the dissociation of other conformations (surface or edge bound). This conclusion is supported by Mulliken charge analysis, which reveals that the positive charge is preferentially located on the nickel atoms in both the parent and fragment ions. In addition, the calculated trivial binding energy of the $[(Cor)_2Ni]^+$ ion indicates that laser desorption leads to a cluster ion better described as an ionic complex between CorNiH and Cor-H.

The investigation of other types of intercalant species is also encouraged, as it will expand the scope of this project and shed light on the fundamental host-guest interactions and their underlying mechanisms. Upon ion intercalation, different host-guest interactions usually induce different intercalation chemistries. New approaches to intercalation include binary or ternary element intercalation, multivalent ion intercalation, and complexed-ion intercalation (20). Further research will deepen the understanding of intercalation chemistry and will guide the exploration of new guests and hosts.

Acknowledgement

PMM thanks the Natural Sciences and Engineering Research Council of Canada for continuing financial support, and the authors thank the JLH Mass Spectrometry Core Facility of the University of Ottawa for the use of the MALDI-TOF instrument.

References

1. Rahman, Md. A., Rahaman, Md. Z, A Review on High- T_c Superconductors and Their Principle Applications. J. Adv. Phys., 4, 87–100 (2015). DOI:10.1166/jap.2015.1175
2. Yao, C., Ma, Y, Superconducting materials: Challenges and opportunities for large-scale applications. IScience, 24, 102541 (2021). doi.org/10.1016/j.isci.2021.102541
3. Kubozono, Y., Eguchi, R., Goto, H., Hamao, S., Kambe, T., Terao, T., Nishiyama, S., Zheng, L., Miao, X., & Okamoto, H. Recent progress on carbon-based superconductors. J. Phys.: Condens. Matt. 28, 334001 (2016). DOI: 10.1088/0953-8984/28/33/334001
4. Dresselhaus, M. S., Dresselhaus, G. Intercalation compounds of graphite. Advances in Physics, 51, 1–186 (2002). DOI:10.1080/00018730110113644
5. Zamani, M., Abbasnejad, M. Optical properties of superconductor-graphene-superconductor junction. Physica C: Superconductivity and Its Applications, 554, 19–26. (2018). doi.org/10.1016/j.physc.2018.09.001
6. Huynh, T. M. D., Hung, G.-S., Gumbs, G., Tran, N. T. T. Fundamental properties of alkali-intercalated bilayer graphene nanoribbons. Phys. Chem. Chem. Phys., 25, 18284–18296 (2023). doi.org/10.1039/D3CP02266H
7. Hannay, N. B., Geballe, T. H., Matthias, B. T., Andres, K., Schmidt, P., MacNair, D. Superconductivity in Graphitic Compounds. Phys. Rev. Lett., 14, 225–226 (1965). DOI: https://doi.org/10.1103/PhysRevLett.14.225
8. Gauzzi, A., Takashima, S., Takeshita, N., Terakura, C., Takagi, H., Emery, N., Hérold, C., Lagrange, P., Loupias, G. Enhancement of Superconductivity and Evidence of Structural Instability in Intercalated Graphite under High Pressure. Phys. Rev. Lett., 98, 067002 (2007). DOI: https://doi.org/10.1103/PhysRevLett.98.067002.
9. Feng, C., Lin, C. S., Fan, W., Zhang, R. Q., van Hove, M. A. Stacking of polycyclic aromatic hydrocarbons as prototype for graphene multilayers, studied using density functional theory augmented with a dispersion term. J. Chem. Phys.131, 194702 (2009). DOI: 10.1063/1.3251785.
10. Lin, Y.-C., Matsumoto, R., Liu, Q., Solís-Fernández, P., Siao, M.-D., Chiu, P.-W., Ago, H., Suenaga, K. Alkali metal bilayer intercalation in graphene. Nature Commun., 15, 425. (2024). https://doi.org/10.1038/s41467-023-44602-3.
11. Wang, X. F., Liu, R. H., Gui, Z., Xie, Y. L., Yan, Y. J., Ying, J. J., Luo, X. G., Chen, X. H. Superconductivity at 5 K in alkali-metal-doped phenanthrene. Nature Commun., 2, 507 (2011). https://doi.org/10.1038/ncomms1513.
12. Wang, X.-Y., Yao, X., Müllen, K. Polycyclic aromatic hydrocarbons in the graphene era. Science China Chemistry, 62, 1099–1144 (2019). https://doi.org/10.1007/s11426-019-9491-2.

13. Cristadoro, A., Räder, H. J., Müllen, K. Clustering of polycyclic aromatic hydrocarbons in matrix-assisted laser desorption/ionization and laser desorption mass spectrometry. Rapid Commun. Mass Spectrom., 21, 2621–2628 (2007). DOI: 10.1002/rcm.3134
14. Pozniak, B. P., Dunbar, R. C. Monomer and Dimer Complexes of Coronene with Atomic Ions. J. Am. Chem. Soc., 119, 10439–10445 (1997). doi.org/10.1021/ja9716259
15. Dunbar, R. C. Binding of Transition-Metal Ions to Curved π Surfaces: Corannulene and Coronene. J. Phys. Chem. A, 106, 9809–9819. (2002). doi.org/10.1021/jp020313b
16. Frisch, M. J.; Trucks, G. W.; Schlegel, H. B.; Scuseria, G. E.; Robb, M. A.; Cheeseman, J. R.; Scalmani, G.; Barone, V.; Petersson, G. A.; Nakatsuji, H.; Li, X.; Caricato, M.; Marenich, A. V.; Bloino, J.; Janesko, B. G.; Gomperts, R.; Mennucci, B.; Hratchian, H. P.; Ortiz, J. V.; Izmaylov, A. F.; Sonnenberg, J. L.; Williams-Young, D.; Ding, F.; Lipparini, F.; Egidi, F.; Goings, J.; Peng, B.; Petrone, A.; Henderson, T.; Ranasinghe, D.; Zakrzewski, V. G.; Gao, J.; Rega, N.; Zheng, G.; Liang, W.; Hada, M.; Ehara, M.; Toyota, K.; Fukuda, R.; Hasegawa, J.; Ishida, M.; Nakajima, T.; Honda, Y.; Kitao, O.; Nakai, H.; Vreven, T.; Throssell, K.; Montgomery Jr., J. A.; Peralta, J. E.; Ogliaro, F.; Bearpark, M. J.; Heyd, J. J.; Brothers, E. N.; Kudin, K. N.; Staroverov, V. N.; Keith, T. A.; Kobayashi, R.; Normand, J.; Raghavachari, K.; Rendell, A. P.; Burant, J. C.; Iyengar, S. S.; Tomasi, J.; Cossi, M.; Millam, J. M.; Klene, M.; Adamo, C.; Cammi, R.; Ochterski, J. W.; Martin, R. L.; Morokuma, K.; Farkas, O.; Foresman, J. B.; Fox, D. J. Gaussian 16 rev. C.01, Wallingford, CT, (2016).
17. West, B., Rodriguez Castillo, S., Sit, A., Mohamad, S., Lowe, B., Joblin, C., Bodi, A., Mayer, P. M. Unimolecular reaction energies for polycyclic aromatic hydrocarbon ions. Phys. Chem. Chem. Phys., 20, 7195–7205 (2018). doi.org/10.1039/C7CP07369K
18. NIST Chemistry Webbook, NIST Standard Reference Database Number 69. National Institute of Standards and Technology: Gaithersburg, MD (2023).
19. Schröder, D., Loos, J., Schwarz, H., Thissen, R., Preda, D. V., Scott, L. T., Caraiman, D., Frach, M. V., Böhme, D. K. Single and Double Ionization of Corannulene and Coronene. Helvetica Chimica Acta, 84, 1625–1634 (2001). DOI:10.1002/1522-2675(20010613)84:6<1625::AID-HLCA1625>3.0.CO;2-0
20. Li, Y., Lu, Y., Adelhelm, P., Titirici, M.-M., Hu, Y.-S. Intercalation chemistry of graphite: alkali metal ions and beyond. Chem. Soc. Rev., 48, 4655–4687 (2019). doi.org/10.1039/C9CS00162J.